ACADEMIC PRESS

Available online at www.sciencedirect.com
SCIENCE DIRECT®

Journal of Catalysis 215 (2003) 271–278

JOURNAL OF CATALYSIS

www.elsevier.com/locate/jcat

Water gas shift reaction for the reformed fuels over Cu/MnO catalysts prepared via spinel-type oxide

Yohei Tanaka,[a] Toshimasa Utaka,[a] Ryuji Kikuchi,[a] Tatsuya Takeguchi,[a] Kazunari Sasaki,[b] and Koichi Eguchi [a,*]

[a] *Department of Energy and Hydrocarbon Chemistry, Graduate School of Engineering, Kyoto University, Yoshida-honmachi, Sakyo-ku, Kyoto 606-8501, Japan*

[b] *Department of Molecular and Material Sciences, Interdisciplinary Graduate School of Engineering Sciences, Kyushu University, 6-1 Kasugakoen, Kasuga-shi, Fukuoka 816-8580, Japan*

Received 24 September 2002; revised 31 December 2002; accepted 13 January 2003

Abstract

Cu/MnO catalysts prepared via reduction of Cu–Mn spinel oxide were investigated for development of active Cu catalysts for the water gas shift reaction (WGSR). A Cu–Mn catalyst active for the WGSR was obtained after high temperature calcination at 900 °C and subsequent reduction. The optimum Cu/Mn ratio for catalytic activity of the Cu–Mn oxide system was 1/2. Nonstoichiometric $Cu_{1.5}Mn_{1.5}O_4$ phase existed stably when copper manganese oxide was calcined above 700 °C. The optimized Cu–Mn spinel showed excellent WGSR activity when a larger percentage of CO was used, as in hydrocarbon reforming. Cu–Mn spinel oxides calcined above 900 °C were easily reduced. This may be responsible for the high activity of the Cu/MnO catalyst. Carbon dioxide in the reformed gas significantly depressed WGSR activity below 200 °C, while CO conversion reached equilibrium at 200 °C in the absence of CO_2.

Keywords: Cu/MnO; $CuMn_2O_4$; Spinel oxide; Water gas shift reaction; CO removal; Reformed gas

1. Introduction

Hydrogen has attracted much attention as one of the most important energy media due to its cleanliness and potential application to various energy conversion processes. Hydrogen has been used in refineries and recently was proposed as a fuel for combustion and fuel cells [1]. In principle, fuel cell systems have higher efficiency of electricity generation than internal combustion engine systems since chemical energy is almost directly converted to electric energy in fuel cells. Polymer electrolyte fuel cells (PEFCs) constitute a promising system for power generation on a small scales [2–5]. PEFCs are operated at low temperature, around 80 °C, and have high energy density suitable for small stationary generators and vehicles.

Since dense storage or liquefaction of hydrogen is possible only at high pressure and/or low temperature, hydrogen storage is an obstacle in use of H_2-fueled PEFCs in automobiles. To solve this problem, on-board reforming of hydrocarbons, methanol, and dimethyl ether has been proposed [1,6]. Recently, hydrocarbons were proposed as a hydrogen source for PEFCs because there exists an infrastructure, such as petroleum stations and city gas pipelines. However, reformed fuels from hydrocarbons contain higher levels of CO than fuels from methanol, e.g., 1–10% CO, due to the thermodynamic equilibrium. Carbon monoxide is irreversibly adsorbed on the Pt electrode of a PEFC, leading to deterioration in cell performance. Therefore, the CO level must be reduced to that allowable for a Pt electrode (10–20 ppm) [7–9].

The water gas shift reaction (WGSR) has been investigated and used in industry [10–13]:

$$H_2O + CO \rightarrow H_2 + CO_2.$$

The reaction temperature is relatively controllable because of the moderately exothermic nature ($\Delta H_{298} = -41.1$ kJ/mol) in contrast to the large exothermic heat for CO oxidation to CO_2 ($\Delta H_{298} = -283$ kJ/mol). Hence, the WGSR is desirable for CO removal from reformed fuels containing high concentrations of CO. The difficulty in removing

* Corresponding author.
E-mail address: eguchi@scl.kyoto-u.ac.jp (K. Eguchi).

0021-9517/03/$ – see front matter
doi:10.1016/S0021-9517(03)00024-1

CO from the reformed gas by the WGSR derives from the following: Since WGSR is exothermic, the lower reaction temperature favors the shift in chemical equilibrium in the forward direction. On the other hand, from a kinetics viewpoint, catalysts are not active enough to reach equilibrium at low temperature. The copper based catalyst for WGSR can be deactivated by H_2O at low temperatures as we have previously reported [14]. Therefore, the optimum reaction temperature is generally found to be between 200 and 250 °C.

We have found out that the Cu–Mn spinel oxide showed excellent WGSR activity comparable to that of conventional $Cu/ZnO/Al_2O_3$ despite its low surface area. Thus, we investigated Cu–Mn spinel oxide with low surface area as a promising catalyst for the WGSR. Cu–Mn spinel oxide was reduced by H_2 in the reformed gas and worked as Cu/MnO [15]. $CuMn_2O_4$, called hopcalite, has been investigated as a CO oxidation catalyst at ambient temperature in applications such as gas masks for miners and also oxidation catalysts for other gas species [16–18].

In this article, effects of preparation conditions, concentrations of gas species, and reduction treatment on the catalytic activity of Cu–Mn spinel oxide for the WGSR in reformed fuels are reported. The effect of the method of preparation of Cu/MnO via spinel-type oxide and the reason for the high activity are also discussed.

2. Experimental

2.1. Preparation and characterization

Copper manganese oxide catalysts and $Cu/ZnO/Al_2O_3$ catalyst were prepared by the coprecipitation method. In the preparation of Cu–Mn spinel oxides, aqueous ammonia and a solution of nitrates (Kishida, analytical grade) were added to a beaker to maintain pH 8. The resultant gel was dried in air at 100 °C for 12 h and precalcined at 400 °C for 1 h to remove nitrate residue. Then the dried powder was calcined at 900 °C for 10 h. The precipitate of $Cu/ZnO/Al_2O_3$ was obtained by adding aqueous ammonia to a solution of nitrates of Cu, Zn, and Al until the precipitate formed at around pH 7. The resultant slurry was dried at 100 °C for 12 h, precalcined at 400 °C for 1 h, and then calcined at 500 °C for 3 h in air.

Surface area of the catalysts was measured by the BET method with N_2 adsorption using a Yuasa Ionics NOVA2200. The crystalline phase of the catalysts was determined by X-ray diffraction (XRD) using a Rigaku RINT1400. To estimate the crystallinity of Cu–Mn spinel oxide, 0.150 g of silicon powder (99.9995% purity, Aldrich) was added to 0.150 g of sample powder as an internal standard material. Crystallinity of spinel oxides is defined as $C_i = 100P_i/P_{\max}$; $P_i = S_i/S_0$, where i represents the calcination temperature of Cu–Mn oxides. S_i is the peak area of (311) diffraction of spinel oxides at $2\theta \approx 36°$, S_0 is the peak area of silicon (111) at $2\theta \approx 28.4°$. $P_{\max}$ is the maximum P_i in P_{500}, P_{700}, P_{900}, and P_{1100}. Temperature-programmed reduction (TPR) was carried out by feeding 10% H_2 in Ar to 25 mg of catalyst sample in a conventional flow reactor without oxidation treatment prior to measurements. The flow rate of the reducing gas was set at 40 ml/min. The temperature of the reactor was raised from room temperature to 800 °C at the rate of 10 K/min. The rate of H_2 consumption was determined by using a thermal conductivity detector and recorded on an on-line personal computer. N_2O titration ($N_2O + 2Cu \rightarrow Cu_2O + N_2$) was implemented at 100 °C by injecting N_2O pulses into a conventional flow reactor. Samples were reduced with 10% H_2/He at 300 °C for 10 min prior to the titration. [Cu]/[Mn] ratios were determined by ICP emission spectrometry (Seiko Instruments, SPS1700HVR) after copper manganese oxides were dissolved in a dilute hydrochloric acid solution.

2.2. Evaluation of catalytic activity

Cu–Mn spinel oxide catalysts were used without prereduction treatment and reduced by H_2 in the feed gas unless otherwise noted. $Cu/ZnO/Al_2O_3$ was reduced at 220 °C for 2 h in a 20% H_2/N_2 stream prior to evaluation of activity. Catalytic activity was examined in a conventional flow reactor at atmospheric pressure in the temperature range 200 to 350 °C and at a constant space velocity of 6400 h^{-1}, using 1.5 ml of catalyst. A model gas after steam reforming of methanol containing H_2, CO, H_2O, CO_2, and N_2 (balance) was supplied to the catalyst bed through mass flow controllers (STEC, SEC-400MK3). The standard composition of the reaction gas was 37.5% H_2, 1.25% CO, 25.0% H_2O, 12.5% CO_2, and N_2 (balance). The gas composition before and after the reaction was analyzed by on-line gas chromatography with a thermal conductivity detector (Shimadzu, GC-8A). A molecular sieve 13X column was used for separation of H_2, O_2, N_2, and CO, and a Porapak Q column for CO_2.

3. Results and discussion

3.1. Effect of calcination temperature

We have reported that Cu–Mn spinel oxide calcined at 900 °C shows excellent WGSR activity for removal of CO in reformed fuels despite its low surface area [15]. Under reducing conditions including a large amount of H_2, the Cu–Mn spinel oxide catalyst is reduced to Cu/MnO. The surface area of Cu–Mn spinel oxide, so-called hopcalite, is very low (≈ 1 m^2/g). It is expected that a decrease in calcination temperature would minimize the loss of surface area and WGSR activity. The calcination temperature of the catalyst was varied from 500 to 1100 °C. Hereafter, Cu–Mn spinel oxide calcined at X °C is denoted as CuMnX ($X = 500, 700$, 900, and 1100).

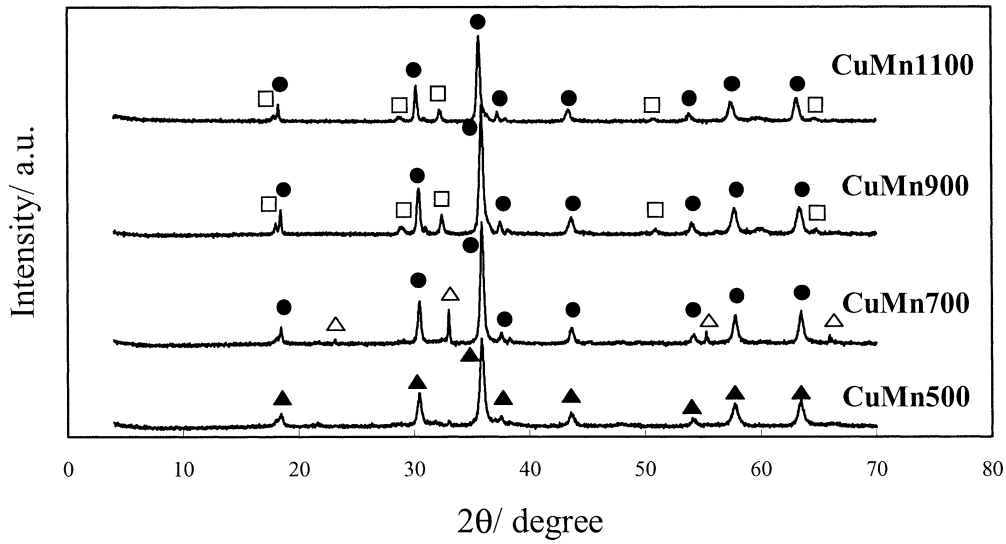

Fig. 1. XRD patterns of CuMnX: (●) $Cu_{1.5}Mn_{1.5}O_4$, (□) Mn_3O_4, (▲) $CuMn_2O_4$, (△) Mn_2O_3.

Table 1
Properties of CuMnX catalysts after calcination

Sample	Calcination temperature (°C)	Crystalline phase	BET surface area (m^2/g)	Crystallinity (%)	Crystallite size[a] (nm)
CuMn500	500	$CuMn_2O_4$	6.6	88	33
CuMn700	700	$Cu_{1.5}Mn_{1.5}O_4$, Mn_2O_3	4.4	100	43
CuMn900	900	$Cu_{1.5}Mn_{1.5}O_4$, Mn_3O_4	0.8	94	32
CuMn1100	1100	$Cu_{1.5}Mn_{1.5}O_4$, Mn_3O_4	0.6	92	37

[a] Crystallite size was obtained for the 311 peak by the Sherrer equation.

Fig. 1 and Table 1 give the crystalline phase, BET surface area, crystallinity, and crystallite size of CuMnX. BET surface area of CuMnX decreased with an increase in calcination temperature. This was because particles of CuMnX shrank as calcination temperature rose. The crystalline phase of CuMn500 was a stoichiometric $CuMn_2O_4$. CuMn700 was composed of a predominant $Cu_{1.5}Mn_{1.5}O_4$ phase and a minor Mn_2O_3 phase. For CuMn900 and CuMn1100 a minor Mn_3O_4 phase was detected together with a predominant $Cu_{1.5}Mn_{1.5}O_4$ phase. This agrees with the results of Hutchings et al., who reported that Cu–Mn solid solution segregated from stoichiometric spinel phase to $Cu_xMn_{3-x}O_4$ and Mn_2O_3 above 600 °C [19]. As shown in Table 1, non-stoichiometric $Cu_{1.5}Mn_{1.5}O_4$ was formed 700 °C. It is probable that the phase separation from stoichiometric $CuMn_2O_4$ occurred above 700 °C, considering the Tamman temperature of Mn_2O_3 (403 °C), which is nearly half of melting point in inorganic materials and indicates the temperature where the solid phase reaction can begin [19,20].

Judging from the results in Table 1, the degree of crystallization of Cu–Mn spinel oxide increased up to 700 °C, then decreased monotonously. The particle size of Cu–Mn spinel oxide also showed a maximum at 700 °C. This suggests that the stoichiometric $CuMn_2O_4$ crystal grew with an increase in calcination temperature up to 700 °C, and, at the same time, decomposition of stoichiometric spinel started around 600–700 °C. The stable phase at this composition is the mixture of $Cu_{1.5}Mn_{1.5}O_4$ and manganese oxide. At 900–1100 °C, reduction of Mn_2O_3 to Mn_3O_4 took place, and the crystallinity and crystallite size of Cu–Mn spinel oxide decreased compared with those of CuMn700.

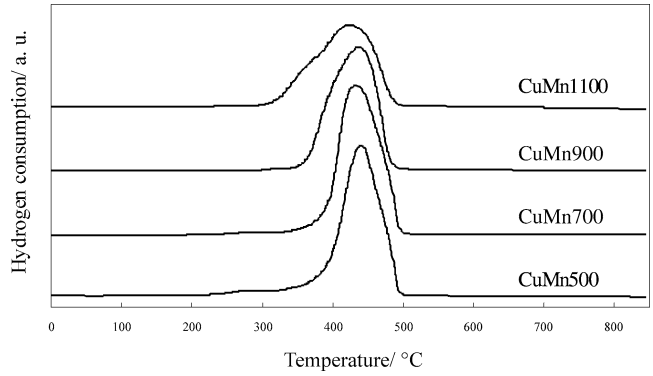

Fig. 2. TPR profiles of CuMnX after calcination. TPR conditions: heating rate, 10 K/min in 10% H_2/Ar.

Fig. 2 comprises TPR profiles of CuMnX after calcination. TPR was carried out without preoxidation. Fig. 3 presents the TPR profiles of CuO, Mn_2O_3, CuMn900, and CuMn900 after WGSR, suggesting that CuO was more reducible than Mn_2O_3. From this figure, the lower temperature region of the reduction peak seen in Fig. 2 was ascribed to

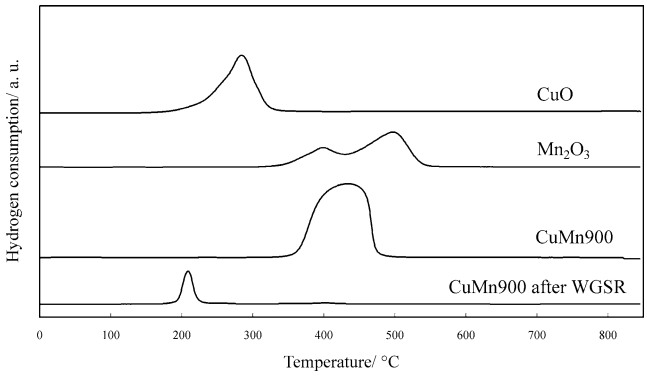

Fig. 3. TPR profiles of CuO, Mn_2O_3, CuMn900, and CuMn900 after the WGSR. TPR conditions: heating rate, 10 K/min in 10% H_2/Ar. WGSR conditions are the same as in Fig. 4.

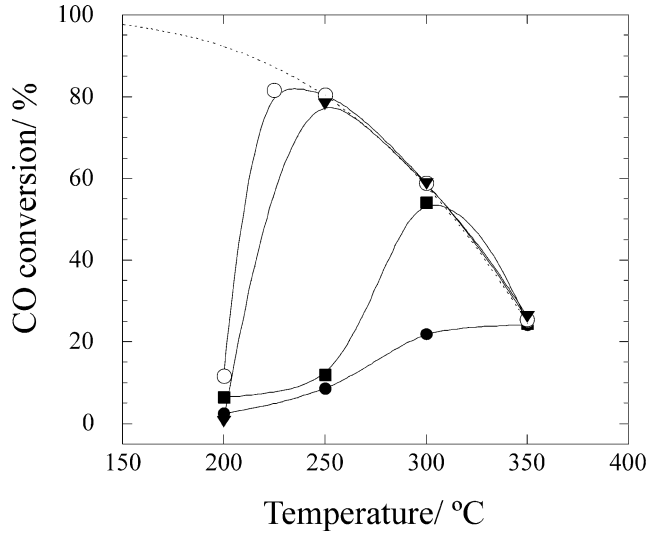

Fig. 4. Catalytic activity of Cu–Mn spinel oxides for WSGR calcined at various temperatures: (●) CuMn500, (■) CuMn700, (○) CuMn900, (▼) CuMn1100, (- - -) equilibrium conversion. Reaction conditions: H_2, 37.5%; CO, 1.25%; H_2O, 25.0%; CO_2, 12.5%; space velocity, 6400 h^{-1}.

reduction of CuO in the spinel lattice, and the higher temperature region, to reduction of Mn_2O_3 to MnO via Mn_3O_4, though it is hard to define a clear boundary between the two regions. As seen in Fig. 2, there was little difference between CuMn500 and CuMn700. The amounts of CuO in CuMn900 and CuMn1100 reduced between 300 and 380 °C were much larger than those in CuMn500 and CuMn700. This suggests that above 900 °C the Cu–Mn spinel oxide is calcined at a higher temperature, the more reducible the spinel is than CuMn500 and CuMn700. It is considered that decomposition or reduction of Cu–Mn spinel oxide to $Cu_{1.5}Mn_{1.5}O_4$ and Mn_3O_4 above 900 °C induces microstructural changes. The porous microstructure may enhance the reducibility of Cu–Mn spinel oxide.

Fig. 4 illustrates the WGSR activity of CuMn*X* as a function of reaction temperature. CuMn900 exhibited maximum activity in the temperature range studied. WGSR activity increased with an increase in calcination temperature up to 900 °C. CuMn1100 showed catalytic activity comparable to that of CuMn900 above 250 °C. It is clear from this result that the WGSR activity of Cu–Mn spinel oxide depended on calcination temperature, and a higher temperature was favorable. After the WGSR, as shown in Fig. 5, the crystalline phase of CuMn*X* was composed mainly of Cu and MnO. Small amounts of Cu_2O or CuO were also detected, which were probably formed by oxidation in air during the XRD measurements in air. In every sample, no peak ascribed to spinel oxide was detected after the WGSR.

Table 2 summarizes Cu particle size of CuMn*X* after the WGSR estimated by N_2O titration. Reduction of CuMn*X* calcined at lower temperatures tended to cause aggregation of Cu particles, leading to low WGSR activity. Although the

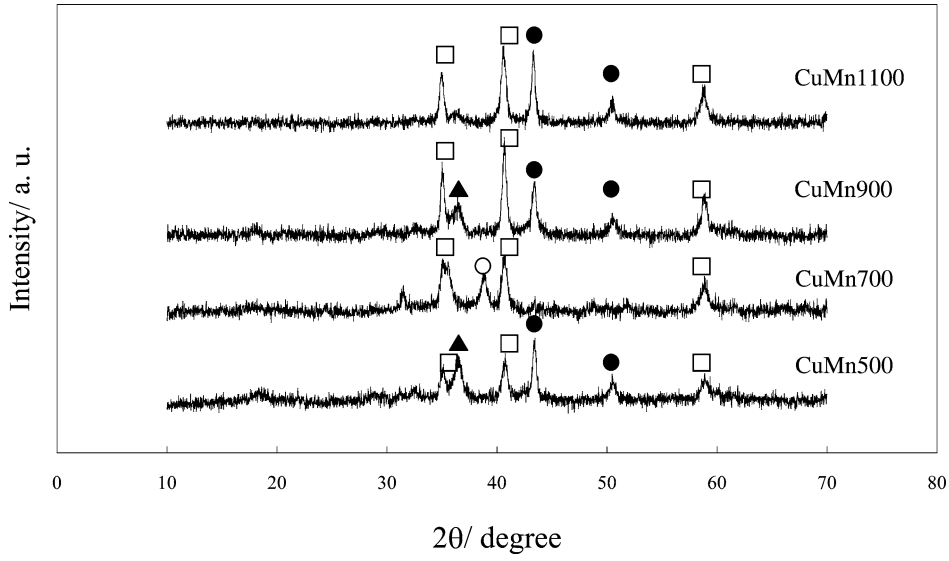

Fig. 5. XRD patterns of CuMn*X* after the WGSR: (●) Cu, (□) MnO, (▲) Cu_2O, (○) CuO. Reaction conditions for the WGSR are the same as in Fig. 4.

Table 2
Properties of CuMnX catalysts after reaction

Sample	Calcination temperature (°C)	Crystalline phase	CO conversion at 250 °C (%)	Cu particle size (nm)
CuMn500	500	Cu, Cu_2O, MnO	8.6	84
CuMn700	700	CuO, MnO	13	44
CuMn900	900	Cu, Cu_2O, MnO	81	42
CuMn1100	1100	Cu, MnO	79	51

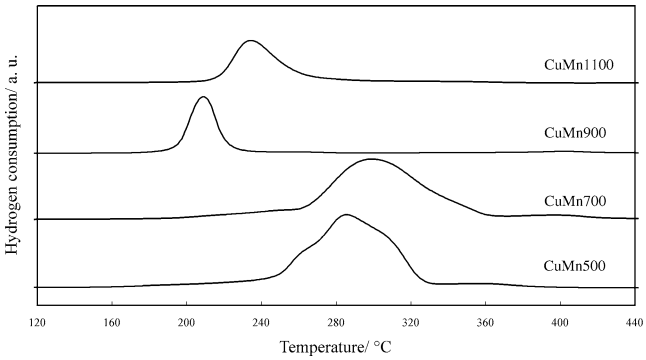

Fig. 6. TPR profiles of CuMnX after the WGSR. TPR conditions: heating rate, 10 K/min in 10% H_2/Ar. WGSR conditions are the same as in Fig. 4.

Cu particle sizes for CuMn700 were comparable to those for CuMn900, catalytic activities for WGSR were quite different, indicating that support strongly affected the active site of Cu particles or WGSR which is discussed later.

To clarify the state of Cu particles, TPR was carried out. Dow et al. have reported that α, β, and γ peaks existed at ca. 160, 210, and 250 °C, respectively, over Cu/γ-Al_2O_3 or Cu/YSZ catalyst [21]. The α and β peaks were ascribed to reduction of highly dispersed Cu species which were not detected by XRD analysis. The γ peak was ascribed to reduction of bulky CuO called isolated Cu species. We also have reported that two Cu species were observed over $Cu/ZnAl_2O_4$ catalyst and one was a Cu dispersed on the support, and the other is an isolated Cu species. According to the report, CuO species dispersed on $ZnAl_2O_4$ were easily reduced [22]. From those results, we can state that highly dispersed CuO_x is reduced at lower temperatures than are bulky CuO species.

Fig. 6 comprises TPR profiles of CuMnX after the WGSR, and in Fig. 3 the TPR profiles for CuO, Mn_2O_3, and CuMn900 are shown in order to assign the peaks in Fig. 6. Only a single peak was detected that can be ascribed to reduction of Cu_2O or CuO in CuMn900 and CuMn1100. In the case of CuMn500 and CuMn700, a shoulder peak was detected at ca. 270 °C, which was ascribable to reduction of relatively dispersed copper oxide species. The peak temperature for the reduction of CuMn900 was the lowest among the catalysts; i.e., the sequence was CuMn900 < CuMn1100 < CuMn500 < CuMn700. It can be said that copper species derived from CuMn900 and CuMn1100 were more highly dispersed on MnO than those from CuMn500 and CuMn700, though CuMn700 showed higher CO conversion than CuMn500 as displayed in Fig. 4.

It can be said, based on the WGSR data, and TPR and XRD measurements, that by reduction of easily reducible CuMn900 and CuMn1100, highly dispersed Cu species are formed and contribute to high CO conversion at 225–250 °C.

3.2. Effect of Cu/Mn molar ratio

From the above results, the optimal calcination temperature of Cu–Mn spinel oxide was estimated to be 900 °C for WGSR activity. In this section, calcination temperature is fixed at 900 °C and the molar ratio of Cu to Mn is varied from 1/8 to 2/1. In Table 3 properties of catalysts are summarized. The catalysts are labeled CuAMnB, where the molar ratio Cu/Mn = A/B. The BET surface area of CuAMnB was ca. 1 m^2/g and tended to decrease with an increase in Mn content. Cu1Mn1, composed of only $Cu_{1.5}Mn_{1.5}O_4$ phase, had a relatively high surface area, probably because the phase was stable at 900 °C. However, impurities such as CuO, Mn_2O_3, and Mn_3O_4 were unstable, resulting in low surface area. Therefore, the BET surface area of CuAMnB depended on the content of $Cu_{1.5}Mn_{1.5}O_4$ structure. This is the reason why Cu1Mn1 exhibited the highest BET surface area among CuAMnB catalysts. The Cu/Mn ratios, which were determined by ICP emission spectroscopy, almost agreed with the nominal ones.

The crystalline phase of CuAMnB was composed mainly of nonstoichiometric $Cu_{1.5}Mn_{1.5}O_4$ and minor Mn_2O_3. When [Cu]/[Mn] = 1/8, Mn_3O_4 (spinel structure) was the predominant phase, while $Cu_{1.4}Mn_{1.6}O_4$ was a minor phase. This result clarified that the nonstoichiometric spinel phase exists stably in the Cu–Mn system once copper manganese is calcined above 600 °C.

Fig. 7 shows WGSR activity over CuAMnB as a function of temperature. Above 250 °C, equilibrium CO conversion for the WGSR is attained over almost all the CuAMnB catalysts. CO conversions increased with an increase in reaction temperature, since the reaction rate limited CO conversion at low temperatures. At 225 °C, the order of WGSR activity was Cu1Mn2 ≈ Cu1Mn1 > Cu1Mn4 > Cu2Mn1 > Cu1Mn8. At 200 °C, the order was Cu1Mn1 > Cu1Mn2 > Cu2Mn1 > Cu1Mn4 > Cu1Mn8. The CO conversion attained over the Cu1Mn2 catalyst was ca. 80%, even at 225 °C. Although Cu1Mn1 showed the highest CO conversion at 200 °C among the catalysts, the value was not enough for CO removal.

Table 3
Properties of CuAMnB catalysts

Sample	Cu/Mn molar ratio[a]	Crystalline phase	BET surface area (m^2/g)	Cu particle size (nm)
Cu2Mn1	2/1.6	$Cu_{1.4}Mn_{1.6}O_4$, CuO	0.9	184
Cu1Mn1	1/0.85	$Cu_{1.5}Mn_{1.5}O_4$	1.4	76
Cu1Mn2 (CuMn900)	0.5/0.43	$Cu_{1.5}Mn_{1.5}O_4$, Mn_3O_4	0.8	42
Cu1Mn4	0.25/0.23	$Cu_{1.5}Mn_{1.5}O_4$, Mn_2O_3	0.7	42
Cu1Mn8	0.125/0.11	Mn_3O_4, $Cu_{1.4}Mn_{1.6}O_4$	0.6	53

[a] Set value/value determined by ICP emission spectrometry. All samples were calcined at 900 °C for 10 h.

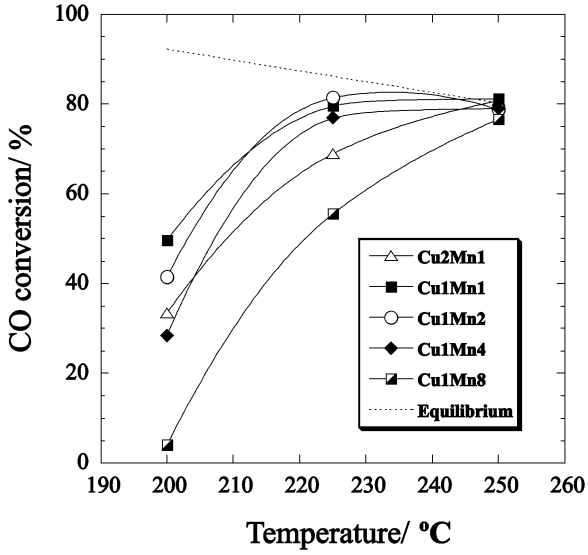

Fig. 7. Catalytic activity of CuAMnB with different A/B ratios at 200–250 °C. Reaction conditions: H_2, 37.5%; CO, 1.25%; H_2O, 25.0%; CO_2, 12.5%; space velocity, 6400 h^{-1}.

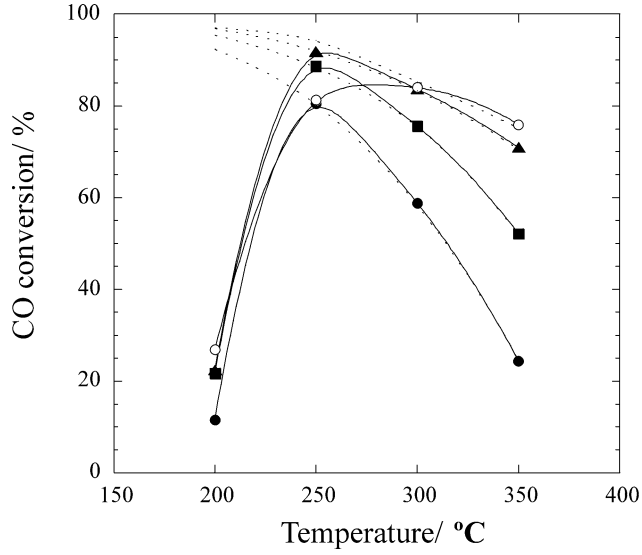

Fig. 8. Temperature dependence of CO conversion for several initial CO concentrations over CuMn900. Initial CO concentration: (●) 1.25%, (■) 2.50%, (▲) 5.00%, (○) 10%. Reaction conditions: H_2, 37.5%; CO, 1.25–10.0%; H_2O, 25.0%; CO_2, 12.5%; space velocity, 6400 h^{-1}.

Cu particle sizes of the samples after the WGSR are listed in Table 3. Cu particle size decreased with an increase in Mn content except for Cu1Mn8. Since the high Cu content led to a high probability of the existence of neighboring Cu atoms in the spinel lattice, Cu species tended to form an agglomerate on reduction with H_2. No obvious correlation could be found between Cu particle size and WGSR activity. In the particle size region 30–100 nm, where a morphological effect would not emerge, TOF tends to be constant and WGSR depends on Cu loading.

It is inferred from the above results that the increase in Cu loadings led to the increase in WGSR activity until Cu/Mn = 1, but excess Cu loading brought about Cu aggregation during reduction of $Cu_{1.5}Mn_{1.5}O_4$ and Mn_3O_4 or Mn_2O_3 to Cu and MnO, which accompanied the decrease in CO conversion. Therefore, the optimum Cu/Mn ratio is considered to be ca. 1/2.

3.3. Dependence on initial CO concentration

From the results in Sections 3.1 and 3.2, CuMn900 (Cu1Mn2) is the optimal catalyst for WGSR activity. We have reported that CuMn900 maintains high and stable WGSR activity in the short-term running test [15]. Recently, hydrocarbons have been proposed as a hydrogen source for PEFCs because there exists an infrastructure, such as petroleum stations and city gas pipelines. When hydrogen is supplied by steam reforming of hydrocarbons, the reformed gas contains much higher CO concentrations than reformed methanol gas. The influence of initial CO concentration on WGSR activity over CuMn900 was investigated.

As shown in Fig. 8, the increase in initial CO concentration up to 5.00% led to the increase in CO conversion in the measured temperature range. CO conversion reached a the maximum at 250 °C in each case except for the initial CO concentration of 10%. CO conversion did not reach equilibrium at 250 °C under the 10% CO condition. This is, as Hutchings and co-workers reported for cobalt oxide-supported copper catalysts, probably because competitive adsorption of CO dominated over that of H_2O on Cu sites under the CO-rich condition. As a result, the relative abundance of surface hydroxyl groups, which is believed to be the key intermediate in oxidation of adsorbed CO, was limited. And regeneration of the Cu sites can be hindered, which is considered to lead to lower CO conversion than equilibrium at 250 °C [23]. Fig. 9 illustrates the outlet CO concentrations from CO conversions in Fig. 8. CO concentration was

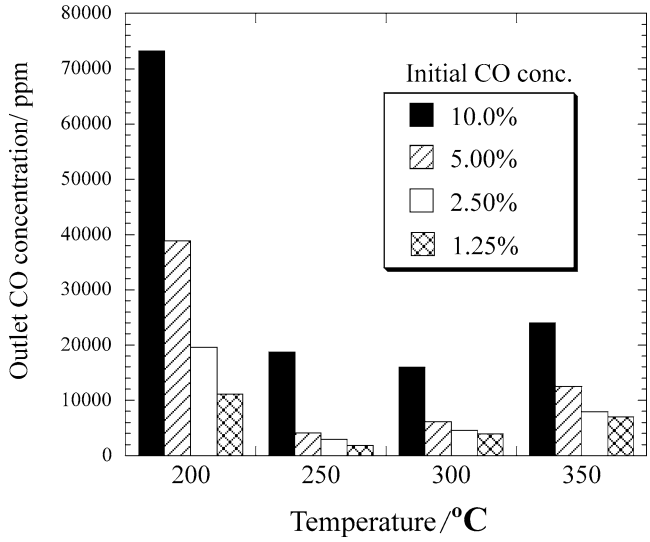

Fig. 9. Outlet CO concentration after the WGSR over CuMn900 supplied with reformed gases at various CO concentrations. Reaction conditions: H_2, 37.5%; CO, 1.25–10.0%; H_2O, 25.0%; CO_2, 12.5%; space velocity, 6400 h^{-1}.

lowered to ca. 4000 ppm at 250 °C over CuMn900 for initial 5.00% CO gas. From this result, it could be said that CuMn900 can be a candidate as a WGSR catalyst to remove relatively high concentrations of CO in reformed hydrocarbons. However, preferential oxidation of CO is still needed after the CO shift reaction to remove residual CO to the level that PEFCs allow.

3.4. Effect of CO_2 on WGSR activity

Since the water gas shift reaction is reversible, CO conversions are influenced by CO_2 and H_2. Although the WGSR has been well investigated, there have been few surveys of WGSRs in concentrated CO_2 and H_2. We have reported that CO_2 suppresses the WGSR over $Cu/ZnO/Al_2O_3$ catalyst [24]. Fig. 10 shows the effect of coexistence of CO_2 in the feed gas. From the thermodynamic equilibrium, the CO conversion decreases in particular at higher temperatures as the initial CO_2 increases. The experimental data agree well with equilibrium conversions above 250 °C. At 200 °C, the WGSR almost reached equilibrium when no CO_2 was included in the reformed gas and 99% CO conversion was obtained, whereas the WGSR was suppressed when more than 6.25% CO_2 was present.

These results suggest that CO_2 coexisting in the reformed gas suppresses CO conversion at low temperatures, even though higher CO conversion is expected from the thermodynamics. It is inferred that the low desorption rate of CO_2 or its high surface coverage at low temperatures brings about low activity at 200 °C in the presence of CO_2. It is clarified that promotion of CO_2 desorption at lower temperatures is one of the keys in developing low temperature WGSR catalysts. The material and surface modification of supports would also affect desorption of CO_2.

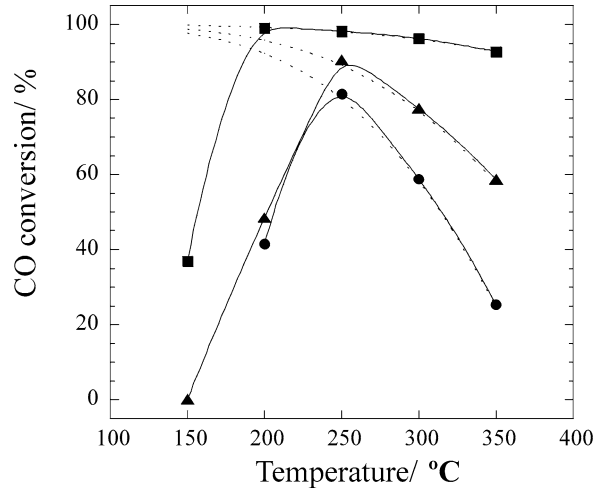

Fig. 10. Temperature dependence of WGSR activity over CuMn900 supplied with various concentrations of CO_2. Reaction conditions: CO_2, (■) 0%, (▲) 6.25%, (●) 12.5%; H_2, 37.5%; CO, 1.25%; H_2O, 25.0%; space velocity, 6400 h^{-1}.

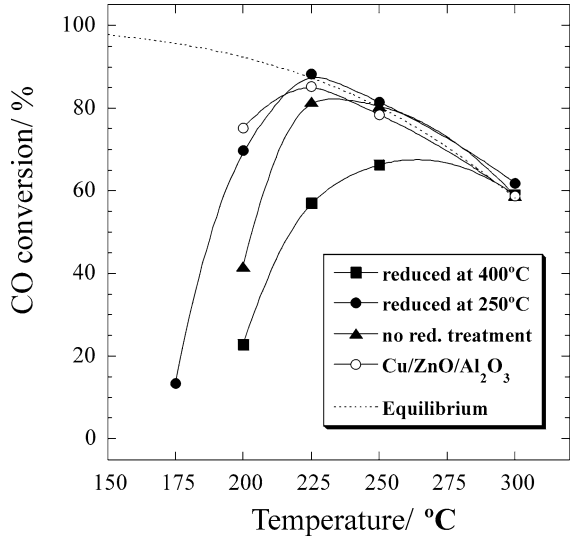

Fig. 11. WGSR activity over CuMn900 after several reduction treatments. Reduction was carried out by feeding 10% H_2/N_2 prior to the WGSR. Reaction conditions: H_2, 37.5%; CO, 1.25%; H_2O, 25.0%; CO_2, 12.5%; space velocity, 6400 h^{-1}.

3.5. Effect of reduction treatment against Cu–Mn spinel oxide on WGSR activity

As discussed in Section 3.1, the Cu–Mn spinel oxide catalyst is reduced in a hydrogen atmosphere or under the reaction conditions. From Fig. 3, it is expected that the reduction of Cu–Mn spinel oxide is facilitated at 350–480 °C. We have reported that reduction at 400 °C degraded the catalytic activity of Cu–Mn spinel oxide [15]. As depicted in Fig. 11, reduction of Cu–Mn spinel oxide at 250 °C prior to the WGSR greatly enhanced CO conversions below 225 °C, and the WGSR reached thermodynamic equilibrium. It was found that CO conversion of Cu–

Mn spinel oxide with reduction treatment at 250 °C is comparable to that of conventional $Cu/ZnO/Al_2O_3$.

Considering the effect of reduction temperature, it is assumed that the mild reduction of Cu–Mn spinel oxide results in high dispersion of Cu on the MnO support. This is probably because Mn dispersed atomically near the Cu sites in the spinel lattice can hinder Cu agglomeration under mild reduction conditions. However, a clear correlation between Cu particle size and WGSR activity was not observed by N_2O titration. This may be because MnO may play a role in CO adsorption on the Cu/MnO surface and promote the WGSR. Xu et al. have reported that addition of MnO into Fe/silicalite catalyst enhances CO adsorption capacity for CO and CO_2 hydrogenation [25, 26]. For CO_2 hydrogenation for hydrocarbon formation, a two-step reaction mechanism involving a reversible WGSR and a Fischer–Tropsch reaction has been suggested [27,28]. Treviño et al. have also proposed that formate may be formed by adsorption of nondissociative CO on the MnO surface of Mn-promoted zeolite Y-supported Rh catalyst for CO hydrogenation [29]. Therefore, in our case, the MnO support itself may contribute to the WGSR as an adsorption site of CO and may be one of the reasons for high WGSR activity despite low surface area.

4. Conclusions

The preparation of Cu/MnO from Cu–Mn spinel oxides and the concentrations of gas species significantly affected the catalytic activity for the water gas shift reaction. Calcination of Cu–Mn spinel oxide at high temperature was favored for promoting the WGSR despite the low BET surface area. The crystallinity of Cu–Mn spinel oxides was at a maximum when the calcination temperature was at 700 °C. Decomposition or reduction of spinel to $Cu_{1.5}Mn_{1.5}O_4$ and Mn_3O_4 is considered to have occurred at 900 and 1100 °C. Cu–Mn spinel oxides calcined above 900 °C showed higher reducibility than those calcined at 500 and 700 °C in TPR measurements. Those results suggest that easily reducible Cu species were highly dispersed and contributed to high CO conversion at low temperatures. This characteristic microstructure was verified by XRD and TPR measurements.

The Cu/Mn ratio of Cu–Mn spinel oxide affected the Cu particle size of Cu/MnO, but the particle size was not directly related to WGSR activity. The optimum Cu/Mn ratio was 1/2. This is probably because in the particle size region 30–100 nm, TOF tends to be constant and WGSR depends on Cu loading. It was confirmed that nonstoichiometric $Cu_{1.5}Mn_{1.5}O_4$ existed stably.

The Cu–Mn spinel oxide in optimized composition showed excellent CO conversion even when a large amount of CO was present, which strongly suggests the potential possibility of this catalyst system for CO removal in reformed hydrocarbon gas. It is expected that MnO species promote the WGSR by adsorbing CO. CO_2 coexisting in reformed gas depressed CO conversion below 200 °C, while CO conversion easily attained equilibrium at 200 °C in the absence of CO_2. The rate of CO_2 desorption is considered to be related to catalytic activity at low temperatures where high CO conversion is attained thermodynamically. Mild reduction treatment against Cu–Mn spinel oxide enhanced WGSR activity.

Acknowledgments

This research was partially supported by Grants-in-Aid for Scientific Research from the Ministry of Education, and also by the New Energy and Industrial Technology Development Organization (NEDO), Japan.

References

[1] J.N. Armor, Appl. Catal. 176 (1999) 159–162.
[2] P.G. Patil, J. Power Sources 37 (1992) 171.
[3] J.C. Amphlett, R.M. Baumert, R.F. Mann, B.A. Peppley, P.R. Roberge, J. Electrochem. Soc. 142 (1995) 1.
[4] L. Clarkin, D. Epp, in: Proceedings of 2nd International Fuel Cell Conference, 1996, p. 370.
[5] G.G. Schere, Solid State Ionics 94 (1997) 249.
[6] V.V. Galvita, G.L. Semin, V.D. Belyaev, T.M. Yurieva, V.A. Sobyanin, Appl. Catal. 216 (2001) 85–90.
[7] S.H. Oh, R.M. Sinkevitch, J. Catal. 142 (1993) 254.
[8] V.M. Schmidt, P. Bröcherhoff, B. Höhlein, R. Menzer, U. Stimming, J. Power Sources 49 (1994) 299.
[9] N. Hashimoto, H. Kudo, J. Adachi, M. Shinagawa, N. Yamada, A. Igarashi, in: Proceedings of 32nd IECEC, 1997.
[10] C.T. Campbell, K.A. Daube, J. Catal. 104 (1987) 109.
[11] G.C. Chinchen, M.S. Spencer, Catal. Today 10 (1991) 293.
[12] A.J. Elliot, R.A. Hadden, J. Tabatabali, K.C. Waugh, F.W. Zemicael, J. Catal. 157 (1995) 153.
[13] H.E. Curry-Hyde, M.S. Wainwright, D.J. Young, Appl. Catal. 77 (1991) 89.
[14] Y. Tanaka, T. Utaka, R. Kikuchi, K. Sasaki, K. Eguchi, Appl. Catal. 238 (2003) 11–18.
[15] Y. Tanaka, T. Utaka, R. Kikuchi, K. Sasaki, K. Eguchi, Appl. Catal. 242 (2003) 285–293.
[16] S. Veprek, D.L. Cocke, S. Kehl, H.R. Oswald, J. Catal. 100 (1986) 250.
[17] P. Porta, G. Moretti, M. Musicanti, A. Nardella, Solid State Ionics 63–65 (1993) 257–267.
[18] G. Fierro, S. Morpurgo, M.L. Jacono, M. Inversi, I. Pettiti, Appl. Catal. 166 (1998) 407–417.
[19] G.J. Hutchings, A.A. Mirzaei, R.W. Joyner, M.R.H. Siddiqui, S.H. Taylor, Appl. Catal. 166 (1998) 149–150.
[20] CRC Handbook of Chemistry and Physics, 74th ed., CRC Press, Boca Raton, FL, 1993–1994.
[21] W.-P. Dow, Y.-P. Wang, T.-J. Huang, J. Catal. 160 (1996) 157–163.
[22] T. Takeguchi, Y. Kani, M. Inoue, K. Eguchi, Catal. Lett. 83 (2002) 50.
[23] G.J. Hutchings, R.G. Copperthwaite, F.M. Gottschalk, R. Hunter, J. Mellor, S.W. Orchard, T. Sangiorgio, J. Catal. 137 (1992) 421.
[24] K. Sekizawa, S. Yano, K. Eguchi, H. Arai, Appl. Catal. 169 (1998) 291–297.
[25] L.Y. Xu, Q.X. Wang, Y.D. Xu, J.S. Huang, Catal. Lett. 25 (1994) 177.
[26] L. Xu, Q. Wang, D. Liang, L. Lin, W. Cui, Y. Xu, Appl. Catal. 173 (1998) 22–25.
[27] M.D. Lee, J.F. Lee, C.S. Chang, T.Y. Dong, Appl. Catal. 72 (1991) 267.
[28] K. Fujimoto, T. Shikada, Appl. Catal. 31 (1987) 13.
[29] H. Treviño, G.D. Lei, W.M.H. Sachtler, J. Catal. 143 (1995) 251.